DALTON
FULL PAPER

Redox routes to arenechromium complexes of two-, three- and four-electron alkynes; structure and bonding in paramagnetic $[Cr(CO)L(\eta\text{-}RC{\equiv}CR)(\eta\text{-arene})]^+$

Christopher J. Adams,[a] Ian M. Bartlett,[a] Neil G. Connelly,*[a] David J. Harding,[a] Owen D. Hayward,[a] Antonio J. Martín,[a] A. Guy Orpen,[a] Michael J. Quayle[a] and Philip H. Rieger[b]

[a] *School of Chemistry, University of Bristol, Bristol, UK BS8 1TS*
[b] *Department of Chemistry, Brown University, Rhode Island, RI 02912, USA*

Received 26th June 2002, Accepted 3rd September 2002
First published as an Advance Article on the web 28th October 2002

X-Ray structural studies on the redox pair $[Cr(CO)_2(\eta\text{-PhC}{\equiv}CPh)(\eta\text{-}C_6Me_5H)]^z$ (z = 0 and 1) show that one-electron oxidation of the neutral complex results in a shortening of the Cr–C_{alkyne} bonds and a lengthening of the Cr–C(O) bonds, consistent with depopulation of a HOMO antibonding with respect to the metal–alkyne interaction. Oxidation leads to an increase in the substitutional lability of the Cr–CO bonds so that $[Cr(CO)_2(\eta\text{-RC}{\equiv}CR)(\eta\text{-}C_6Me_6)]^+$ (R = Ph or C_6H_4OMe-*p*) reacts with Lewis bases to give $[Cr(CO)L(\eta\text{-RC}{\equiv}CR)(\eta\text{-}C_6Me_6)]^+$ {L = CNXyl, $P(OMe)_3$ and $P(OCH_2)_3CEt$}, X-ray studies on which show a rotation of the alkyne to align with the remaining Cr–CO bond. ESR spectroscopic studies on $[Cr(CO)L(\eta\text{-RC}{\equiv}CR)(\eta\text{-}C_6Me_6)]^+$ show delocalisation of the unpaired electron onto the alkyne ligand, consistent with its description as a three-electron donor. The cations $[Cr(CO)L(\eta\text{-RC}{\equiv}CR)(\eta\text{-}C_6Me_6)]^+$ undergo both one-electron reduction and oxidation, and chemical oxidation of $[Cr(CO)\{P(OCH_2)_3CEt\}(\eta\text{-}p\text{-}MeOC_6H_4C{\equiv}CC_6H_4OMe\text{-}p)(\eta\text{-}C_6Me_6)]^+$ with $AgPF_6$ gives the dication $[Cr(CO)\{P(OCH_2)_3CEt\}(\eta\text{-}p\text{-}MeOC_6H_4C{\equiv}CC_6H_4OMe\text{-}p)(\eta\text{-}C_6Me_6)]^{2+}$. Thus the two-electron alkyne of $[Cr(CO)_2(\eta\text{-RC}{\equiv}CR)(\eta\text{-}C_6Me_6)]$ is converted into the four-electron alkyne of $[Cr(CO)L(\eta\text{-RC}{\equiv}CR)(\eta\text{-}C_6Me_6)]^{2+}$ by an ECE (E = electrochemical, C = chemical) process in which all of the intermediates have been fully characterised.

Introduction

In our studies of the redox-activation of metal–alkyne complexes[1] we have provided preliminary results[2] of the structural characterisation of the redox pair $[Cr(CO)_2(\eta\text{-PhC}{\equiv}CPh)(\eta\text{-}C_6Me_5H)]^z$ (z = 0 and 1); the shortening of the Cr–C_{alkyne} bonds on oxidation was consistent with removal of an electron from a HOMO antibonding with respect to the metal–alkyne bond. We now show how this oxidation process, in leading to a stronger metal–alkyne bond and weaker metal–carbonyl bonds, results in a change in the substitutional reactivity of $[Cr(CO)_2(\eta\text{-RC}{\equiv}CR)(\eta\text{-}C_6Me_6)]$ (R = Ph or C_6H_4OMe-*p*). Whereas the alkyne is displaced from $[Cr(CO)_2(\eta\text{-RC}{\equiv}CR)(\eta\text{-}C_6Me_6)]$ by two-electron donor ligands, L, such as isocyanides and phosphites, to give $[Cr(CO)_2L(\eta\text{-}C_6Me_6)]$,[3] carbonyl substitution occurs with the monocation $[Cr(CO)_2(\eta\text{-RC}{\equiv}CR)(\eta\text{-}C_6Me_6)]^+$, affording $[Cr(CO)L(\eta\text{-RC}{\equiv}CR)(\eta\text{-}C_6Me_6)]^+$, X-ray structural studies on which {R = Ph, L = CNXyl (Xyl = 2,6-dimethylphenyl) or $P(OMe)_3$; R = C_6H_4OMe-*p*, L = CNXyl} show the effect of L on metal–alkyne bonding. The monocations $[Cr(CO)L(\eta\text{-RC}{\equiv}CR)(\eta\text{-}C_6Me_6)]^+$ also undergo one-electron oxidation, to the dications $[Cr(CO)L(\eta\text{-RC}{\equiv}CR)(\eta\text{-}C_6Me_6)]^{2+}$. Hence, the two-electron alkyne of $[Cr(CO)_2(\eta\text{-RC}{\equiv}CR)(\eta\text{-}C_6Me_6)]$ is converted to a four-electron alkyne in $[Cr(CO)L(\eta\text{-RC}{\equiv}CR)(\eta\text{-}C_6Me_6)]^{2+}$ by an ECE (E = electrochemical, C = chemical) series of reactions, similar to those relating d^5 $[M(CO)_2(\eta\text{-RC}{\equiv}CR)Tp']$ {M = Mo or W, Tp′ = hydrotris(3,5-dimethylpyrazolyl)borate} to d^2 $[MX_2(\eta\text{-RC}{\equiv}CR)Tp']^+$ (X = halide) in a 'redox family tree'.[4]

Results and discussion

The synthesis of $[Cr(CO)_2(\eta\text{-RC}{\equiv}CR)(\eta\text{-arene})][PF_6]$

The $[PF_6]^-$ salts of the dicarbonyls $[Cr(CO)_2(\eta\text{-PhC}{\equiv}CPh)(\eta\text{-}C_6Me_5H)]^+$ **1**$^+$, $[Cr(CO)_2(\eta\text{-RC}{\equiv}CR)(\eta\text{-}C_6Me_6)]^+$ (R = Ph **2**$^+$, C_6H_4OMe-*p* **3**$^+$) (required for X-ray structural studies of **1**$^+$ and **3**$^+$ and the synthetic studies described below) were prepared by oxidising the corresponding neutral complexes $[Cr(CO)_2(\eta\text{-RC}{\equiv}CR)(\eta\text{-arene})]$[5] using $[Fe(\eta\text{-}C_5H_5)_2][PF_6]$ rather than $[NO][PF_6]$.[6]

The X-ray structures of $[Cr(CO)_2(\eta\text{-PhC}{\equiv}CPh)(\eta\text{-}C_6Me_5H)]$ **1**, $[Cr(CO)_2(\eta\text{-PhC}{\equiv}CPh)(\eta\text{-}C_6Me_5H)][PF_6]\cdot CH_2Cl_2$ **1**$^+[PF_6]^-\cdot CH_2Cl_2$ and $[Cr(CO)_2(\eta\text{-}p\text{-MeOC}_6H_4C{\equiv}CC_6H_4\text{-OMe-}p)(\eta\text{-}C_6Me_6)][PF_6]$ **3**$^+[PF_6]^-$

The structures of **1** and **1**$^+$ are shown in Figs. 1 and 2 and important bond distances and angles for these complexes, as

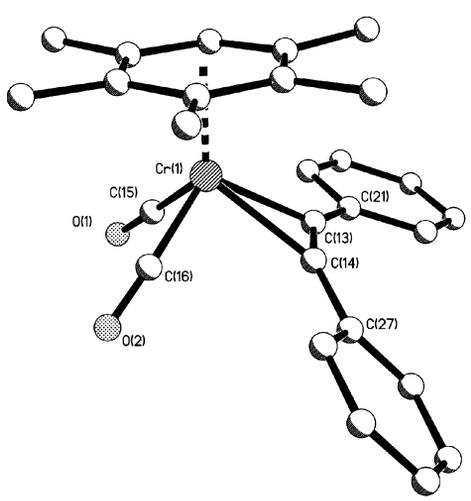

Fig. 1 The molecular structure of $[Cr(CO)_2(\eta\text{-PhC}{\equiv}CPh)(\eta\text{-}C_6Me_5H)]$ **1**. Hydrogen atoms have been omitted for clarity.

DOI: 10.1039/b206177p

Table 1 Important bond lengths (Å) and angles (°) for $[Cr(CO)L(\eta\text{-}RC{\equiv}CR)(\eta\text{-arene})]^z$ (z = 0 or 1)

	1	**1**$^+$	**3**$^+$	**4**$^+$	**6**$^{+\,a}$		**7**$^+$
Cr–C(13)	2.136(4)	2.034(6)	2.031(4)	2.037(3)	2.028(6)	2.023(6)	2.037(4)
Cr–C(14)	2.144(6)	2.044(7)	2.059(4)	2.087(3)	2.067(6)	2.056(6)	2.088(4)
C(13)–C(14)	1.259(3)	1.262(10)	1.276(6)	1.277(4)	1.269(8)	1.267(8)	1.275(5)
Cr–C(15)	1.823(3)	1.880(6)	1.895(5)	1.847(3)	1.832(8)	1.822(8)	1.840(4)
Cr–C(16)	1.816(4)	1.869(8)	1.865(5)	1.959(3)	—	—	1.962(4)
C(15)–O(1)	1.166(3)	1.140(8)	1.142(5)	1.154(3)	1.159(7)	1.167(7)	1.151(4)
C(16)–O(2)	1.166(3)	1.131(9)	1.146(6)	—	—	—	—
Cr(16)–N(1)	—	—	—	1.171(4)	—	—	1.156(5)
Cr–P(1)	—	—	—	—	2.298(2)	2.289(2)	—
C(13)–Cr–C(14)	34.2(1)	36.1(3)	36.3(2)	36.1(1)	36.1(2)	36.2(2)	36.0(1)
C(14)–C(13)–C(21)	150.3(2)	145.0(6)	146.2(4)	145.5(3)	142.2(6)	143.6(6)	142.6(4)
C(27)–C(14)–C(13)	149.1(2)	146.2(6)	143.3(4)	148.3(3)	145.7(6)	142.4(6)	144.6(4)
C(15)–Cr–C(16)	81.5(1)	91.5(4)	92.2(2)	89.1(1)	—	—	91.2(2)
C(15)–Cr–P(1)	—	—	—	—	86.1(2)	85.1(2)	—
C(15)–Cr–C(13)	85.3(2)	84.3(3)	83.8(2)	107.5(1)	110.0(3)	109.4(3)	108.3(2)
C(15)–Cr–C(14)	103.9(2)	104.0(3)	102.4(2)	74.9(1)	77.0(3)	75.3(3)	73.7(2)
C(16)–Cr–C(13)	107.9(2)	106.5(3)	109.1(2)	87.3(1)	—	—	85.6(2)
C(16)–Cr–C(14)	82.5(1)	76.1(3)	77.5(2)	101.7(1)	—	—	95.9(1)
P(1)–Cr–C(13)	—	—	—	—	87.5(1)	87.6(2)	—
P(1)–Cr–C(14)	—	—	—	—	99.6(1)	96.3(2)	—
β^b	59.0, 43.9	58.9, 33.5	30.7, 61.0	26.1	25.1	20.1	16.5

^{a} Contains two independent molecules in the asymmetric unit. ^{b} See text for definition.

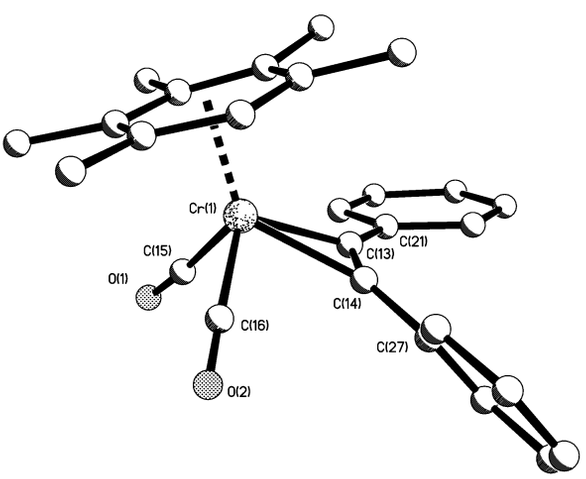

Fig. 2 The molecular structure of $[Cr(CO)_2(\eta\text{-}PhC{\equiv}CPh)(\eta\text{-}C_6Me_5H)]^+$ **1**$^+$. Hydrogen atoms have been omitted for clarity.

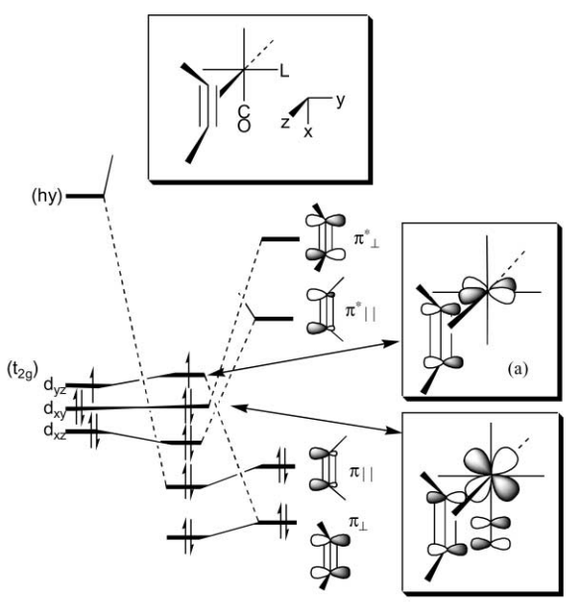

Fig. 3 Schematic MO diagram for pseudo-octahedral d^5 complexes $[Cr(CO)L(\eta\text{-alkyne})(\eta\text{-}C_6H_6)]^+$ or $[Mo(CO)L(\eta\text{-alkyne})(\eta^5\text{-}C_5H_5)]$. The three *fac* sites are shown as vacant. Orbital (a), the SOMO for the d^5 species, is the HOMO for d^6 and the LUMO for d^4 complexes. The alkyne orientation shown is that observed for d^4 and d^5 species with L ≠CO.

well as **3**$^+$, are given in Table 1. Most of the following discussion is based on structural comparisons between the redox pair **1** and **1**$^+$; the structure of the d^5 dicarbonyl species **3**$^+$ is generally very similar to that of **1**$^+$.

The three structures are broadly similar in that the metal is in a pseudo-octahedral environment with the arene occupying three facial sites and the alkyne and two carbonyl ligands the remaining positions; the alkyne C≡C bond lies nearly parallel to the plane of the arene ring.

The most striking change on oxidation of **1** to **1**$^+$ is the shortening of the $Cr–C_{alkyne}$ bonds, by *ca.* 0.1 Å. The mean value of Cr(1)–C(13) and Cr(1)–C(14) is 2.140(6) Å in **1** and 2.039(7) Å in **1**$^+$; the mean value for **3**$^+$ [2.045(4) Å] is similar to that of **1**$^+$. The shortening of the $Cr–C_{alkyne}$ bond can be rationalised in terms of the MO diagram for the pseudo-octahedral d^5 complex $[CrL_2(\eta\text{-alkyne})(\eta\text{-}C_6H_6)]^+$ (or $[MoL_2(\eta\text{-alkyne})(\eta^5\text{-}C_5H_5)]$) (Fig. 3); one-electron oxidation of **1** half depopulates the HOMO, which is antibonding with respect to the $M–C_{alkyne}$ bonds. [Note that although this orbital is bonding with respect to the alkyne carbon–carbon bond, the expected lengthening of this bond on oxidation is not detectable; C(13)–C(14) is 1.262(10) Å in **1**$^+$ and 1.259(3) Å in **1** {*cf.* 1.276(6) Å in **3**$^+$}].

It is interesting to note the very different structural effects of one-electron oxidation on metal–alkene and metal–alkyne bonds. The shortening of the $Cr–C_{alkyne}$ bonds noted above is mirrored by that of the $Mo–C_{alkyne}$ bonds (again by *ca.* 0.1 Å) on oxidation of d^5 $[Mo(CO)_2(PhC{\equiv}CPh)Tp']$ to d^4 $[Mo(CO)_2(PhC{\equiv}CPh)Tp']^+$,[2] and the $Ru–C_{alkyne}$ bonds (by 0.03–0.04 Å) in

the redox pair $[Ru(acac)_2(o\text{-}PhC{\equiv}CC_6H_4NMe_2)]^z$ (z = 0 and 1)[7]}. In marked contrast, the metal–C_{alkene} bond is lengthened (by *ca.* 0.17 Å) in the Mo(alkene) fragment when $[Mo_2(\mu\text{-}C_8Me_8)(\eta\text{-}C_5H_5)_2]$ (Fig. 4) is oxidised to $[Mo_2(\mu\text{-}C_8Me_8)(\eta\text{-}C_5H_5)_2]^+$,[8] and by *ca.* 0.09 Å in the Ru^{II}/Ru^{III} redox pair $[Ru(acac)_2(o\text{-}CH_2{=}CHC_6H_4NMe_2)]^z$ (z = 0 and 1).[9] The Dewar–Chatt–Duncanson model[10] for metal–alkene bonding accounts for the difference in that oxidation will result in depopulation of a metal–alkene π-bonding orbital (either directly, or indirectly by depopulation of a metal orbital). Oxidation therefore inhibits metal-to-alkene π-back donation and the metal–alkene bond is weakened and lengthened.

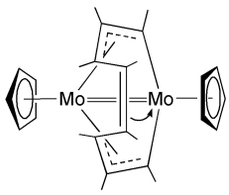

Fig. 4 $[Mo_2(\mu\text{-}C_8Me_8)(\eta^5\text{-}C_5H_5)_2]$.

Complexes **1** and $\mathbf{1}^+$ can be described, formally at least, in terms of their metal oxidation states and d-configurations {*i.e.* Cr(0), d^6; Cr(I), d^5 respectively}. However, it is more instructive, and perhaps more realistic given the delocalised bonding within such complexes, to describe them in terms of the bonding mode of the alkyne ligand. Thus, full occupancy of the HOMO for **1**, and of both the bonding and antibonding combinations of the $\pi_\perp$ alkyne orbital with the appropriate metal orbital (see Fig. 3), is consistent with the description of the alkyne as a net two-electron donor. Removal of one electron from the HOMO, to give $\mathbf{1}^+$, thus results in the alkyne acting as a net three-electron donor.

The strengthening of the metal–alkyne bonds on oxidation (as implied by the shorter Cr–C_{alkyne} bonds) is accompanied by a weakening of the Cr–CO bonds, shown not only (indirectly) by the increase in ν(CO) of *ca.* 120 cm^{-1} but also in the lengthening of Cr–C(15) and Cr–C(16), which average 1.820(3) Å in **1** and 1.875(8) Å in $\mathbf{1}^+$ [and 1.880(5) Å in $\mathbf{3}^+$]; the C–O bonds C(15)–O(1) and C(16)–O(2) are also shortened, on average from 1.166(3) Å in **1** to 1.136(9) Å in $\mathbf{1}^+$ [and 1.144(5) Å in $\mathbf{3}^+$]. The effect of strengthening the M–C_{alkyne} bonds and weakening the M–CO bonds on the substitutional chemistry of the redox pair **1** and $\mathbf{1}^+$ is explored below.

Other structural changes are observed on oxidation of **1** to $\mathbf{1}^+$. Thus, the angle C(15)–Cr–C(16) increases by *ca.* 10°, from 81.50(13)° **1** to 91.5(4)° $\mathbf{1}^+$. In other examples where small OC–M–CO angles are observed, minor electronic factors are responsible. For example, EHMO calculations[11] show that the acute OC–M–CO angle of 82.9° for $[W(CO)_2(PhC{\equiv}CMe)Tp']^+$ results in a minor stabilisation of the HOMO and destabilisation of the LUMO orbitals.

There is also a change in the alkyne bend-back angle on oxidation; the average of the angles C(21)–C(13)–C(14) and C(13)–C(14)–C(27) is 149.7(2)° in **1** but 145.6(6)° in $\mathbf{1}^+$ and 144.8(4)° in $\mathbf{3}^+$. This bending implies rehybridisation at the contact carbons which, in turn, facilitates the M–C_{alkyne} σ bond and in-plane back-bonding; the $\pi_\perp$ interaction should be essentially invariant with the bend-back angle.

The torsion angle C(27)–C(14)–C(13)–C(21) of −0.4(6)° in **1** demonstrates perfect *cis*-bent geometry of the diphenyl alkyne, yet in $\mathbf{1}^+$ the same angle is −8.8(2)° showing a modest twist away from planar geometry.

One final aspect of the structures of **1** and $\mathbf{1}^+$ is important with respect to those of $[Cr(CO)(CNXyl)(\eta\text{-}PhC{\equiv}CPh)(\eta\text{-}C_6Me_6)][PF_6]$ $\mathbf{4}^+[PF_6]^-$, $[Cr(CO)\{P(OMe)_3\}(\eta\text{-}PhC{\equiv}CPh)(\eta\text{-}C_6Me_6)][PF_6]$ $\mathbf{6}^+[PF_6]^-$, and $[Cr(CO)(CNXyl)(\eta\text{-}p\text{-}MeOC_6H_4C{\equiv}CC_6H_4OMe\text{-}p)(\eta\text{-}C_6Me_6)][PF_6]$ $\mathbf{7}^+[PF_6]^-$ (see below), namely the alkyne orientation.

EHMO studies[12] on the model complex $[Mo(CO)_2(HC{\equiv}CH)(\eta\text{-}C_5H_5)]^z$ predict that for d^4 or d^6 configurations (z = 1 and −1 respectively) the alkyne will align parallel to the cyclopentadienyl plane, as found in the d^6 species **1** and $[Re(CO)_2(PhC{\equiv}CPh)(\eta\text{-}C_5H_5)]$.[13] Given that the fragments $[Mo(CO)_2(\eta\text{-}C_5H_5)]^-$ and $[Cr(CO)_2(\eta\text{-arene})]$ are isolobal, little or no change is expected, or indeed found, in the alkyne orientation when **1** is oxidised to $\mathbf{1}^+$. By contrast, there is a significant change in the alkyne orientation on CO substitution in $\mathbf{1}^+$ (see below).

The synthesis of $[Cr(CO)L(\eta\text{-}RC{\equiv}CR)(\eta\text{-arene})][PF_6]$ {L = CNXyl, $P(OCH_2)_3CEt$ and $P(OMe)_3$}

As noted above, one-electron oxidation of $[Cr(CO)_2(\eta\text{-}RC{\equiv}CR)(\eta\text{-}C_6Me_6)]$ leads to a weakening of the Cr–CO bonds, a strengthening of the Cr–C_{alkyne} bonds, and thus to a remarkable change in reaction pattern. Rather than alkyne displacement by donor ligands, L, as observed for $[Cr(CO)_2(\eta\text{-}RC{\equiv}CR)(\eta\text{-}C_6Me_6)]$ (to give $[Cr(CO)_2L(\eta\text{-}C_6Me_6)]$),[3] oxidation leads to carbonyl substitution and the formation of $[Cr(CO)L(\eta\text{-}RC{\equiv}CR)(\eta\text{-}C_6Me_6)]^+$.

The reaction of $[Cr(CO)_2(\eta\text{-}PhC{\equiv}CPh)(\eta\text{-}C_6Me_6)][PF_6]$, $\mathbf{2}^+[PF_6]^-$ or $[Cr(CO)_2(\eta\text{-}p\text{-}MeOC_6H_4C{\equiv}CC_6H_4OMe\text{-}p)(\eta\text{-}C_6Me_6)][PF_6]$, $\mathbf{3}^+[PF_6]^-$ in CH_2Cl_2 with the phosphites $P(OCH_2)_3CEt$ and $P(OMe)_3$ and the isocyanide CNXyl yielded red or deep red solutions containing $[Cr(CO)L(\eta\text{-}PhC{\equiv}CPh)(\eta\text{-}C_6Me_6)]^+$ {L = CNXyl, $\mathbf{4}^+$; $P(OCH_2)_3CEt$, $\mathbf{5}^+$; or $P(OMe)_3$, $\mathbf{6}^+$} or $[Cr(CO)L(\eta\text{-}p\text{-}MeOC_6H_4C{\equiv}CC_6H_4OMe\text{-}p)(\eta\text{-}C_6Me_6)]^+$ {L = CNXyl, $\mathbf{7}^+$; $P(OCH_2)_3CEt$, $\mathbf{8}^+$; or $P(OMe)_3$, $\mathbf{9}^+$}. Addition of *n*-hexane and partial evaporation of the solvent *in vacuo* gave dark red to purple precipitates of the $[PF_6]^-$ salts which were purified by allowing a concentrated solution of the complex in CH_2Cl_2 to diffuse into *n*-hexane at −20 °C. The products were then characterised by elemental analysis and IR (Table 2) and ESR spectroscopy (Table 3), cyclic voltammetry (Table 2) and, in the cases of $[Cr(CO)(CNXyl)(\eta\text{-}PhC{\equiv}CPh)(\eta\text{-}C_6Me_6)][PF_6]$ $\mathbf{4}^+[PF_6]^-$, $[Cr(CO)\{P(OMe)_3\}(\eta\text{-}PhC{\equiv}CPh)(\eta\text{-}C_6Me_6)][PF_6]$ $\mathbf{6}^+[PF_6]^-$, and $[Cr(CO)(CNXyl)(\eta\text{-}p\text{-}MeOC_6H_4C{\equiv}CC_6H_4OMe\text{-}p)(\eta\text{-}C_6Me_6)][PF_6]$ $\mathbf{7}^+[PF_6]^-$, by X-ray crystallography.

The IR spectra of $\mathbf{4}^+$–$\mathbf{9}^+$ show the effect of the ligand, L, in that for a given alkyne substituent, Ph or $C_6H_4OMe\text{-}p$, ν(CO) is in the order CNXyl > $P(OCH_2)_3CEt$ > $P(OMe)_3$, in agreement with the suggestion that the 'pinned-back' phosphite $P(OCH_2)_3CEt$ is a better π-acceptor than $P(OMe)_3$ because of its smaller O–P–O angles.[14] For a given ligand, L, ν(CO) is higher in energy, by *ca.* 5–7 cm^{-1}, when R = Ph; for the dicarbonyls **2** and **3**, and $\mathbf{2}^+$ and $\mathbf{3}^+$, the difference is *ca.* 10–12 cm^{-1}. (These trends are also reflected in the electrochemical results described below which also reveal that the effect of R depends on the redox process involved.)

The X-ray structures of $[Cr(CO)(CNXyl)(\eta\text{-}PhC{\equiv}CPh)(\eta\text{-}C_6Me_6)][PF_6]$ $\mathbf{4}^+[PF_6]^-$, $[Cr(CO)\{P(OMe)_3\}(\eta\text{-}PhC{\equiv}CPh)(\eta\text{-}C_6Me_6)][PF_6]$ $\mathbf{6}^+[PF_6]^-$, and $[Cr(CO)(CNXyl)(\eta\text{-}p\text{-}MeOC_6H_4C{\equiv}CC_6H_4OMe\text{-}p)(\eta\text{-}C_6Me_6)][PF_6]$ $\mathbf{7}^+[PF_6]^-$

The structures of the cations $\mathbf{4}^+$, $\mathbf{6}^+$ and $\mathbf{7}^+$ are shown in Figs. 5–7 respectively. Important bond lengths and angles are given in Table 1.

In general, the structures of these d^5 species, $[Cr(CO)L(\eta\text{-}RC{\equiv}CR)(\eta\text{-}C_6Me_6)]^+$, are similar to those of $\mathbf{1}^+$ and $\mathbf{3}^+$ although replacing one CO ligand of the dicarbonyl cations by L leads to the remaining Cr–CO bond of $\mathbf{4}^+$, $\mathbf{6}^+$ and $\mathbf{7}^+$ being shorter (1.82–1.85 Å) than those of $[Cr(CO)_2(\eta\text{-}PhC{\equiv}CPh)(\eta\text{-}C_6Me_5H)]^+$ $\mathbf{1}^+$ (1.87 Å) (because of increased Cr-to-CO π-back bonding). However, the structures of $[Cr(CO)L(\eta\text{-}RC{\equiv}CR)(\eta\text{-}C_6Me_6)]^+$ differ in important detail from that of $\mathbf{1}^+$.

As noted above, the C≡C bond of the alkyne in $\mathbf{1}^+$ and $\mathbf{3}^+$ lies approximately parallel to the plane of the arene ring. However,

Table 2 Analytical, IR spectroscopic and electrochemical data for $[Cr(CO)L(\eta\text{-}RC{\equiv}CR)(\eta\text{-}C_6Me_6)][PF_6]$

Complex	Colour	Yield (%)	Analysis (%)[a]			IR[b]/cm^{-1}		E_o'[c]/V	
			C	H	N	ν(CN)	ν(CO)	Ox.[d]	Red.[e]
$[Cr(CO)_2(\eta\text{-}PhC{\equiv}CPh)(\eta\text{-}C_6Me_6)]$ **2**[f]	—	—	—	—	—	—	1900, 1821	—	—
$[Cr(CO)_2(\eta\text{-}PhC{\equiv}CPh)(\eta\text{-}C_6Me_6)]^+$ **2**$^+$[f]	—	—	—	—	—	—	2023, 1975	1.20	−0.18
$[Cr(CO)_2(\eta\text{-}p\text{-}MeOC_6H_4C{\equiv}CC_6H_4OMe\text{-}p)(\eta\text{-}C_6Me_6)]$ **3**[f]	—	—	—	—	—	—	1889, 1811	—	—
$[Cr(CO)_2(\eta\text{-}p\text{-}MeOC_6H_4C{\equiv}CC_6H_4OMe\text{-}p)(\eta\text{-}C_6Me_6)]^+$ **3**$^+$[f]	—	—	—	—	—	—	2011, 1965	0.89	−0.24
$[Cr(CO)(CNXyl)(\eta\text{-}PhC{\equiv}CPh)(\eta\text{-}C_6Me_6)]^+$ **4**$^+$	red-black	57	62.4 (62.1)	5.6 (5.4)	2.1 (2.0)	2110 br	1952	0.91[g]	−0.58
$[Cr(CO)\{P(OCH_2)_3CEt\}(\eta\text{-}PhC{\equiv}CPh)(\eta\text{-}C_6Me_6)]^+$ **5**$^+$	dark red	70	54.3 (54.5)	5.3 (5.4)	—	—	1945	0.78	−0.67
$[Cr(CO)\{P(OMe)_3\}(\eta\text{-}PhC{\equiv}CPh)(\eta\text{-}C_6Me_6)]^+$ **6**$^+$	dark red	69	51.1 (51.1)[h]	5.4 (5.3)	—	—	1929	0.76	−0.75
$[Cr(CO)(CNXyl)(\eta\text{-}p\text{-}MeOC_6H_4C{\equiv}CC_6H_4OMe\text{-}p)(\eta\text{-}C_6Me_6)]^+$ **7**$^+$	red-black	32	59.7 (60.3)	5.6 (5.5)	1.8 (1.9)	2105 br	1945	0.67	−0.64
$[Cr(CO)\{P(OCH_2)_3CEt\}(\eta\text{-}p\text{-}MeOC_6H_4C{\equiv}CC_6H_4OMe\text{-}p)(\eta\text{-}C_6Me_6)]^+$ **8**$^+$	red-purple	57	49.7 (49.6)[i]	5.2 (5.2)	—	—	1940	0.56	−0.73
$[Cr(CO)\{P(OMe)_3\}(\eta\text{-}p\text{-}MeOC_6H_4C{\equiv}CC_6H_4OMe\text{-}p)(\eta\text{-}C_6Me_6)]^+$ **9**$^+$	red-purple	39	47.6 (47.5)[i]	5.3 (5.2)	—	—	1923	0.53	−0.82
$[Cr(CO)\{P(OCH_2)_3CEt\}(\eta\text{-}p\text{-}MeOC_6H_4C{\equiv}CC_6H_4OMe\text{-}p)\ (\eta\text{-}C_6Me_6)]^{2+}$ **8**$^{2+}$	purple	61	41.7 (42.5)[i]	4.4 (4.5)	—	—	2005	0.56[j]	−0.73

[a] Calculated values in parentheses, all as $[PF_6]^-$ salts. [b] Strong absorptions in CH_2Cl_2; br = broad. [c] In CH_2Cl_2; potentials relative to the saturated calomel electrode, calibrated *vs.* the $[Fe(\eta\text{-}C_5Me_5)_2]^+/[Fe(\eta\text{-}C_5Me_5)_2]$ couple (at −0.08 V) unless stated otherwise. [d] Reversible, diffusion-controlled, one-electron oxidation to $[Cr(CO)L(\eta\text{-}RC{\equiv}CR)(\eta\text{-}C_6Me_6)]^{2+}$. [e] Reversible, diffusion-controlled, one-electron reduction to $[Cr(CO)L(\eta\text{-}RC{\equiv}CR)(\eta\text{-}C_6Me_6)]$. [f] Data from ref. 6. [g] Incompletely reversible at 2.0 V s^{-1}; E_o' is the average of the oxidation and reduction peak potentials, $(Ep)ox$ and $(Ep)_{red}$, at 500 mV s^{-1}. [h] Analysed as a 0.25 CH_2Cl_2 solvate. [i] Analysed as a 1 : 1 CH_2Cl_2 solvate. [j] Calibrated against the $[Fe(\eta\text{-}C_5H_4COMe)_2]^+/[Fe(\eta\text{-}C_5H_4COMe)_2]$ couple (at 0.97 V).

Table 3 ESR spectroscopic data for $[Cr(CO)L(\eta\text{-}RC{\equiv}CR)(\eta\text{-}C_6Me_6)]^+$ in CH_2Cl_2–thf (1 : 2)[a], and Cr 3d contribution to the SOMO

Complex	Isotropic spectrum[b]			Anisotropic spectrum[c]										
	g_{iso}	$<A^{Cr}>$	$<A^{P}>$	g_1	g_2	g_3	g_{ave}	A_1(Cr)	A_2(Cr)	A_3(Cr)	$A_1(^{31}P)$	$A_2(^{31}P)$	$A_3(^{31}P)$	ρ^{3d}
4$^+$	1.993[d]	15.1	—	1.974	1.998	2.010	1.994	28.3	7.0[e]	10.0	—	—	—	0.67
5$^+$	1.994	15.0	24.2	1.975	1.997	2.010	1.994	28.1	6.7[e]	9.8	27.0	21.9	28.1	0.67
6$^+$	1.993	15.1	27.7	1.974	1.997	2.010	1.994	28.5(7)[f]	6.5[e]	10.2	29.7	25.6	31.0	0.68
7$^+$	1.994[g]	14.9	—	1.976[h]	1.997	2.009	1.994	[i]	[i]	[i]	—	—	—	—
8$^+$	1.994	14.6	23.7	1.976	1.996	2.010	1.994	27.6(1)	6.5[e]	9.7	26.3	21.3	27.4	0.66
9$^+$	1.993	14.8	27.2	1.974	1.997	2.007	1.993	28.3(7)[f]	6.3[e]	10.0	29.5	25.0	30.4	0.69

[a] Hyperfine couplings in 10^{-4} cm^{-1}. [b] At 240 K unless stated otherwise. [c] At 100 K unless stated otherwise. [d] At 290 K. [e] Computed from isotropic coupling. [f] Large uncertainty probably due to non-coincidence of *g*- and *A*-axes. [g] At room temperature. [h] At 77 K. [i] Not determined.

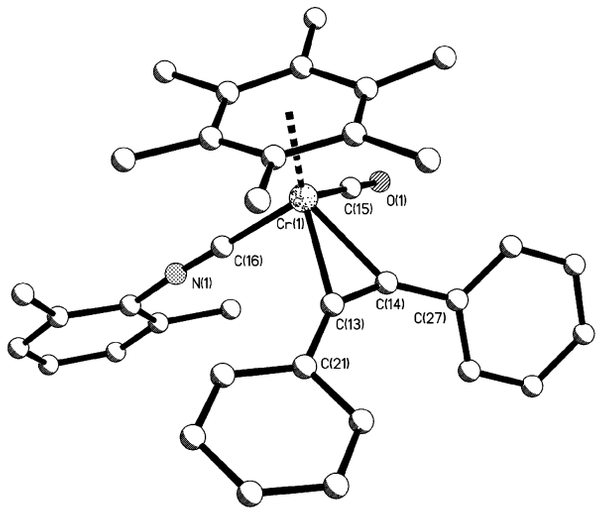

Fig. 5 The molecular structure of $[Cr(CO)(CNXyl)(\eta\text{-}PhC{\equiv}CPh)(\eta\text{-}C_6Me_6)]^+$ **4**$^+$. Hydrogen atoms have been omitted for clarity.

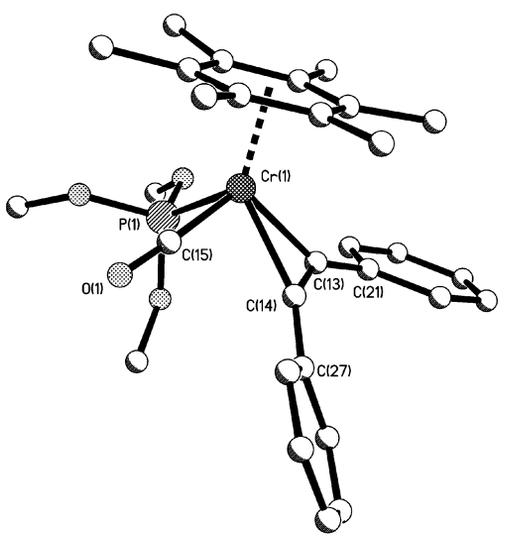

Fig. 6 The molecular structure of $[Cr(CO)\{P(OMe)_3\}(\eta\text{-}PhC{\equiv}CPh)(\eta\text{-}C_6Me_6)]^+$ **6**$^+$. Hydrogen atoms have been omitted for clarity.

substitution of one carbonyl ligand by L results in the C≡C bond lying more nearly parallel to the remaining carbonyl ligand of **4**$^+$–**7**$^+$. The extent of alignment is given by β, the magnitude of the smallest torsion angle, C(15)–Cr(1)–C(14)–C(13) (or its equivalent) between the C≡C vector and the Cr–C(O) vector. In the case of **1**, $\beta = 43.9°$, for **1**$^+$, $\beta = 33.5°$, and for **3**$^+$, $\beta = 30.7°$, while for **4**$^+$ (26.2°), **6**$^+$ (20.1 and 25.1°) and **7**$^+$ (16.5°) β is smaller.

EHMO studies[15] on the model complexes $[Mo(CO)(PH_3)(HC{\equiv}CH)(\eta\text{-}C_5H_5)]^z$ (z = 1, −1) indicated that, unlike in the dicarbonyls, the alkyne orientation depends on the metal d-electron configuration. For the d^6 model complex ($z = -1$) the HOMO has primarily metal d_{yz} character. Thus, to achieve effective overlap of the alkyne $\pi_\parallel$* and metal d_{yz} orbitals, the alkyne must align parallel to the less good π-acceptor, *i.e.* parallel to the Mo–P bond (see Fig. 8). In contrast, in the d^4 complex ($z = 1$) the alkyne aligns with the carbonyl, thereby also allowing donation from the alkyne $\pi_\perp$ orbital into the vacant metal d_{yz} orbital (as shown in Fig. 3). For $[Cr(CO)L(\eta\text{-}RC{\equiv}CR)(\eta\text{-}C_6Me_6)]^+$, with a d^5 configuration, the alkyne aligns with the carbonyl ligand and the structure more nearly adopts the orientational preference of a d^4 rather than a d^6 complex. Apparently, the half-filled d_{yz} orbital may also accept significant electron density from the alkyne $\pi_\perp$ orbital, contributing to the observed alkyne orientation.

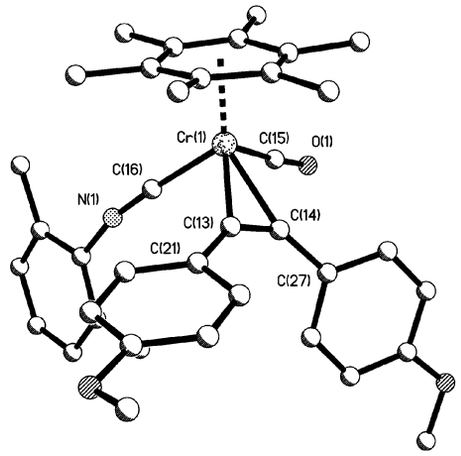

Fig. 7 The molecular structure of $[Cr(CO)(CNXyl)(\eta\text{-}p\text{-}MeOC_6H_4C{\equiv}CC_6H_4OMe\text{-}p)(\eta\text{-}C_6Me_6)]^+$ **7**$^+$. Hydrogen atoms have been omitted for clarity.

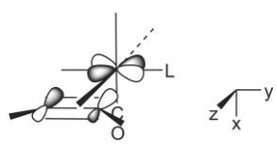

Fig. 8 The HOMO of $[Mo(CO)L(\eta\text{-alkyne})(\eta^5\text{-}C_5H_5)]^-$.

ESR spectroscopic studies of $[Cr(CO)L(\eta\text{-}RC{\equiv}CR)(\eta\text{-}C_6Me_6)][PF_6]$

The cations $[Cr(CO)_2(\eta\text{-}RC{\equiv}CR')(\eta\text{-}C_6Me_6)]^+$ (R = R′ = C_6H_4OMe-*p* or CO_2Me; R = Ph, R′ = H) show[16,17] narrow ESR spectra and *g*-values very close to that of the free electron (g_e = 2.0023) implying substantial delocalisation of electron spin density onto the alkyne. Indeed, hyperfine coupling to the alkynic hydrogen of $[Cr(CO)_2(\eta\text{-}PhC{\equiv}CH)(\eta\text{-}C_6Me_6)]^+$ (4.2 G) showed[16] that as much as 40% of the unpaired electron spin density is located on the alkyne (leading to an alternative description of the ligand, at least formally, as a 'coordinated alkyne radical'). By contrast, the phosphine complexes $[Cr(CO)_2(PR_3)(\eta\text{-}C_6Me_6)]^+$ show comparitively broad ESR spectra and *g*-values much greater than that of a free electron indicating a metal-based 'radical'.[3] ESR spectroscopy was therefore used to investigate whether the electronic structure of $[Cr(CO)L(\eta\text{-}RC{\equiv}CR)(\eta\text{-}C_6Me_6)]^+$ is more like that of $[Cr(CO)_2(\eta\text{-}RC{\equiv}CR)(\eta\text{-}C_6Me_6)]^+$ or $[Cr(CO)_2(PR_3)(\eta\text{-}C_6Me_6)]^+$.

The anisotropic spectra were recorded at 100 K in CH_2Cl_2–thf (1 : 2). The samples were then warmed in approximately 20 K steps until isotropic spectra were observed. The isotropic and anisotropic spectra of $[Cr(CO)\{P(OMe)_3\}(\eta\text{-}PhC{\equiv}CPh)(\eta\text{-}C_6Me_6)]^+$ **6**$^+$, as a representative example, are shown in Figs. 9 and 10 respectively; the ESR parameters for **4**$^+$–**9**$^+$ are listed in Table 3.

The spectra of the six complexes are remarkably similar. The isotropic parameters are $\langle g \rangle = 1.993 \pm 0.001$ and $\langle A^{Cr} \rangle = (14.9 \pm 0.3) \times 10^{-4}$ cm^{-1}; for the two $P(OMe)_3$ complexes, $\langle A^P \rangle = (27.5 \pm 0.4) \times 10^{-4}$ cm^{-1}, and for the two $P(OCH_2)_3CEt$ complexes $\langle A^P \rangle = (23.9 \pm 0.3) \times 10^{-4}$ cm^{-1}. The anisotropic parameters are also similar: a rhombic *g*-matrix with principal values 1.975 ± 0.001, 1.997 ± 0.001, 2.009 ± 0.001, an approximately axial phosphorus hyperfine matrix with the unique (smallest) value corresponding to the middle *g*-value, and an approximately axial chromium hyperfine matrix with the unique (largest) value corresponding to the smallest *g*-value.

The spectra appear to be consistent with previous ESR spectroscopic studies on other Cr(I) and Mn(II) low-spin d^5 piano-stool complexes.[3,18] For example, as a result of '*g*-strain', features corresponding to the largest *g*-value are generally broader than the other features in the present spectra; this

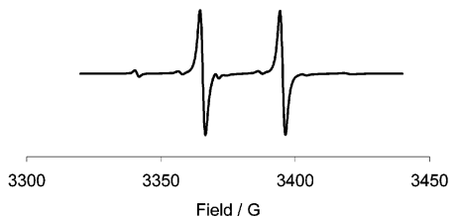

Fig. 9 The isotropic ESR spectrum of $[Cr(CO)\{P(OMe)_3\}(\eta\text{-}PhC{\equiv}CPh)(\eta\text{-}C_6Me_6)]^+$ **6**$^+$ at 240 K, in CH_2Cl_2–thf (1 : 2).

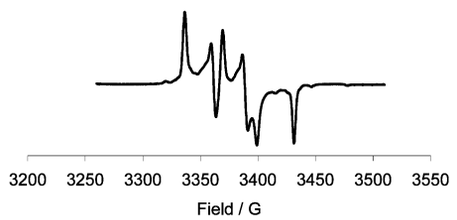

Fig. 10 The anisotropic ESR spectrum of $[Cr(CO)\{P(OMe)_3\}(\eta\text{-}PhC{\equiv}CPh)(\eta\text{-}C_6Me_6)]^+$ **6**$^+$ at 100 K, in CH_2Cl_2–thf (1 : 2).

phenomenon has been attributed to the sensitivity of g_{max} to small variations in L–M–L′ bond angles and the consequent appearence of a range of g_{max} values in a frozen solution. There are, however, several notable differences: (i) here two *g*-components are smaller than g_e, whereas previous complexes had only one small *g*-component; (ii) here the phosphorus hyperfine anisotropy is on the order of 5–6 × 10^{-4} cm^{-1}, whereas the previous complex had anisotropies less than half this magnitude; (iii) chromium hyperfine satellites have not been observed in previous spectra. In the Mn complexes the principal axes of the *g*- and A^{Mn}-matrices were displaced by 20° or more. Here the data are not sufficiently complete to determine non-coincidence angles, but there is clear evidence in the case of the $P(OMe)_3$ complexes, **6**$^+$ and **9**$^+$, that this complication applies to the present spectra.

The chromium hyperfine anisotropy can be used to estimate the Cr 3d contribution to the SOMOs in the present complexes. Assuming an effective single d_{yz}-type orbital, the anisotropy is given by

$$A_{||} - \langle A \rangle = (4/7)P\rho$$

where $P = -34.36 \times 10^{-4}$ cm^{-1}.[19] With the understanding that matrix axis non-coincidence can seriously perturb this calculation, the computed Cr 3d contributions are remarkably constant (Table 3) and very similar to Mn 3d contributions (0.66–0.73) in $[Mn(CO)_2(PR_3)L]$ (L = $\eta\text{-}C_5H_5$ or η^5-cyclohexadienyl).[18]

In previous work on $[Cr(CO)_2L(\eta\text{-}C_6Me_6)]^+$ (L = phosphine or phosphite),[3] two origins were considered for ^{31}P hyperfine anisotropy: dipole–dipole coupling with spin density on Cr, and dipolar coupling with spin density on phosphorus. In the first mechanism, the anisotropy is expected to be proportional to $1/r_{Cr-P}$.[3] For a typical phosphite ligand with r_{Cr-P} = 2.3 Å, and ρ^{3d} = 0.67, an anisotropy of about 1.8 × 10^{-4} cm^{-1} is expected. The observed anisotropy, of the order of 4 × 10^{-4} cm^{-1} for the $P(OMe)_3$ complexes and 6.0 × 10^{-4} cm^{-1} for the $P(OCH_2)_3CEt$ complexes, suggests that the latter ligand is the better π-acceptor, in agreement with electrochemical and IR spectroscopic results.

Electrochemistry

Each of the CVs of **4**$^+$–**9**$^+$, at a platinum electrode in CH_2Cl_2, shows two diffusion-controlled one-electron waves, one oxidation (to **4**$^{2+}$–**9**$^{2+}$) and one reduction (to **4**–**9**) (Table 2). The waves are chemically reversible in all cases except for the oxidation of **4**$^+$ where the peak current ratio, $(i_p)_{red}/(i_p)_{ox}$, remains less than 1.0 even at a scan rates of 2.0 V s^{-1}.

Compared with the redox potentials of **2**$^+$ and **3**$^+$, carbonyl substitution by L shifts the $E^{o'}$ values more negative by *ca.* 0.30–0.45 and 0.40–0.60 V for the oxidation and reduction processes respectively. The potentials for both such processes depend on the nature of L, in the order $E^{o'}$ = CNXyl > $P(OCH_2)_3CEt$ > $P(OMe)_3$, reflecting relative ligand donor–acceptor properties {and in accord with the trend in *ν*(CO) and the ESR spectroscopic analysis, see above}.

Of more note, however, are the effects of the alkyne substituent on potential. Thus, for pairs of complexes with R = Ph and $C_6H_4OMe\text{-}p$ {*e.g.* the dicarbonyls **2**$^+$ and **3**$^+$ and the $P(OMe)_3$ complexes **6**$^+$ and **9**$^+$}, the latter are oxidised more readily, by *ca.* 0.23–0.31 V, and the former are more readily reduced, by *ca.* 0.06 V. The small difference in the potentials for the one-electron reduction contrasts markedly with the much larger difference in the potentials for the formation of the dications. The ability of the methoxy substituents of the alkyne *p*-$MeOC_6H_4C{\equiv}CC_6H_4OMe\text{-}p$ to delocalise positive charge onto the alkyne more effectively may explain this difference. Thus, the dications **7**$^{2+}$–**9**$^{2+}$ may be stabilised by the mesomeric effect of the alkyne substituents whereas such stabilisation of the neutral complexes, formed on reduction, would be minimal.

On the basis of the electrochemical studies noted above, $[Cr(CO)L(\eta\text{-}RC{\equiv}CR)(\eta\text{-}C_6Me_6)]^+$ should be easy both to reduce and oxidise. Surprisingly, therefore, IR spectroscopy indicated that $[Co(\eta\text{-}C_5H_5)_2]$ did not reduce **7**$^+$–**9**$^+$ to the neutral complexes $[Cr(CO)L(\eta\text{-}p\text{-}MeOC_6H_4C{\equiv}CC_6H_4OMe\text{-}p)(\eta\text{-}C_6Me_6)]$. However, treatment of $[Cr(CO)\{P(OCH_2)_3CEt\}(\eta\text{-}p\text{-}MeOC_6H_4C{\equiv}CC_6H_4OMe\text{-}p)(\eta\text{-}C_6Me_6)]^+$ **8**$^+$ with $AgPF_6$ in CH_2Cl_2 resulted in a deep purple solution with *ν*(CO) = 2005 cm^{-1}, an increase in energy of 65 cm^{-1} consistent with the formation of the dication **8**$^{2+}$. Addition of *n*-hexane then resulted in the precipitation of a purple solid which was characterised, after purification, as the 1 : 1 CH_2Cl_2 solvate $[Cr(CO)\{P(OCH_2)_3CEt\}(\eta\text{-}p\text{-}MeOC_6H_4C{\equiv}CC_6H_4OMe\text{-}p)(\eta\text{-}C_6Me_6)][PF_6]_2{\cdot}CH_2Cl_2$ **8**$^{2+}$2$[PF_6]^-{\cdot}CH_2Cl_2$ by elemental analysis and by cyclic voltammetry (Table 2) which shows two reduction waves at the same potentials as those of the oxidation and reduction waves of **8**$^+$.

The isolation of $[Cr(CO)\{P(OCH_2)_3CEt\}(\eta\text{-}p\text{-}MeOC_6H_4C{\equiv}CC_6H_4OMe\text{-}p)(\eta\text{-}C_6Me_6)][PF_6]_2$ therefore completes a series of reactions in which the two-electron alkyne of $[Cr(CO)_2(\eta\text{-}p\text{-}MeOC_6H_4C{\equiv}CC_6H_4OMe\text{-}p)(\eta\text{-}C_6Me_6)]$ (**3**, d^6) is converted to a four-electron alkyne in the d^4 dication *via* an ECE mechanism, *i.e.* by oxidation of **3** to **3**$^+$, carbonyl substitution of **3**$^+$ by $P(OCH_2)_3CEt$ to give **8**$^+$, and oxidation of **8**$^+$ to **8**$^{2+}$.

Conclusions

A comparison of the structures of $[Cr(CO)_2(\eta\text{-}PhC{\equiv}CPh)(\eta\text{-}C_6Me_5H)]$ **1** and $[Cr(CO)_2(\eta\text{-}PhC{\equiv}CPh)(\eta\text{-}C_6Me_5H)][PF_6]$ **1**$^+$ shows a shortening of the $M\text{–}C_{alkyne}$ bonds by *ca.* 0.1 Å, consistent with (i) the alkyne changing from a two- to a three-electron donor on oxidation, and (ii) EHMO calculations which indicate that the HOMO in d^6 $[Cr(CO)_2(RC{\equiv}CR)(\eta\text{-}C_6H_6)]$ is antibonding with respect to the $M\text{–}C_{alkyne}$ bonds. By contrast, the metal–carbonyl bonds are lengthened on oxidation, consistent with reduced Cr to CO π-back-bonding.

The changes in metal–alkyne and metal–carbonyl bonding on oxidation have a marked effect on reactivity. Thus, whereas neutral $[Cr(CO)_2(RC{\equiv}CR)(\eta\text{-}C_6Me_6)]$ undergoes substitution of the alkyne by L, the cation $[Cr(CO)_2(RC{\equiv}CR)(\eta\text{-}C_6Me_6)]^+$ undergoes CO substitution to give the paramagnetic cations $[Cr(CO)L(\eta\text{-}RC{\equiv}CR)(\eta\text{-}C_6Me_6)]^+$ {L = CNXyl, $P(OCH_2)_3CEt$ and $P(OMe)_3$; R = Ph and $C_6H_4OMe\text{-}p$}.

Structural studies on $[Cr(CO)L(\eta\text{-}PhC{\equiv}CPh)(\eta\text{-}C_6Me_6)][PF_6]$ {L = CNXyl and $P(OMe)_3$} and $[Cr(CO)(CNXyl)(\eta\text{-}p\text{-}$

$MeOC_6H_4C{\equiv}CC_6H_4OMe$-*p*)(η-$C_6Me_6$)][$PF_6$] revealed that the alkyne aligns approximately parallel to the carbonyl ligand. The ESR spectra of the paramagnetic cations are similar to those of [$Cr(CO)_2$(η-RC≡CR)(η-C_6Me_6)]$^+$, indicating the unpaired electron spin density to be delocalised extensively on to the alkyne.

Electrochemical studies show that carbonyl substitution by an isocyanide or phosphite ligand results in easier oxidation of [Cr(CO)L(η-RC≡CR)(η-C_6Me_6)]$^+$, to [Cr(CO)L(η-RC≡CR)-(η-C_6Me_6)]$^{2+}$, than [$Cr(CO)_2$(η-RC≡CR)(η-C_6Me_6)]$^+$. Indeed, chemical oxidation of [Cr(CO){$P(OCH_2)_3CEt$}(η-*p*-MeO-$C_6H_4C{\equiv}CC_6H_4OMe$-*p*)(η-$C_6Me_6$)]$^+$ **8**$^+$ yields the isolable salt [Cr(CO){$P(OCH_2)_3CEt$}(η-*p*-$MeOC_6H_4C{\equiv}CC_6H_4OMe$-*p*)-(η-$C_6Me_6$)][$PF_6$]$_2$.

Experimental

The preparation, purification and reactions of the complexes described were carried out under an atmosphere of dry nitrogen using dried, distilled and deoxygenated solvents; reactions were monitored by IR spectroscopy where necessary. Unless stated otherwise complexes were purified by dissolution in CH_2Cl_2, filtration of the solution through Celite, addition of *n*-hexane to the filtrate and reduction of the volume of the mixture *in vacuo* to induce precipitation.

The compounds [$Cr(CO)_3$(η-C_6Me_6)],[20] [$Cr(CO)_2$-(η-RC≡CR)(η-C_6Me_6)] (R = Ph, C_6H_4OMe-*p*),[5] [$Cr(CO)_2$-(η-RC≡CR)(η-arene)][PF_6] (R = Ph, C_6H_4OMe-*p*)[6] and [Fe-(η-C_5H_5)$_2$][PF_6][21] were prepared by published methods.

IR spectra were recorded on a Nicolet 5ZDX FT spectrometer. X-Band ESR spectra were recorded on a Bruker 300ESP spectrometer equipped with a Bruker variable temperature accessory and a Hewlett-Packard 5350B microwave frequency counter. The field calibration was checked by measuring the resonance of the dpph radical before each series of spectra. Electrochemical studies were carried out using an EG&G model 273A potentiostat in conjunction with a three-electrode cell. The auxiliary electrode was a platinum wire and the working electrode a platinum disc (1.6 or 2.0 mm diameter). The reference was an aqueous saturated calomel electrode separated from the test solution by a fine porosity frit and an agar bridge saturated with KCl. Solutions were 1.0×10^{-3} mol dm^{-3} in the test compound and 0.1 mol dm^{-3} in [NBu^n_4][PF_6] as the supporting electrolyte in CH_2Cl_2. Under the conditions used for voltammetry, $E^{o'}$ for the one-electron oxidation of [Fe(η-C_5Me_5)$_2$], added to the test solution as an internal calibrant, is −0.08 V. ($E^{o'}$ for the one-electron oxidation of [Fe(η-C_5H_4COMe)$_2$], used as the calibrant for the CV of complex **8**$^{2+}$, which would oxidise [Fe(η-C_5Me_5)$_2$], is 0.97 V under the same experimental conditions.) Microanalyses were carried out by the staff of the Microanalysis Service of the School of Chemistry, University of Bristol.

Syntheses

[$Cr(CO)_2$(η-*p*-$MeOC_6H_4C{\equiv}CC_6H_4OMe$-*p*)(η-$C_6Me_6$)][$PF_6$] 3$^+$[$PF_6$]$^-$. To a stirred solution of [$Cr(CO)_2$(η-*p*-$MeOC_6$-$H_4C{\equiv}CC_6H_4OMe$-*p*)(η-C_6Me_6)] (100 mg, 0.197 mmol) in CH_2Cl_2 (25 cm^3) was added [Fe(η-C_5H_5)$_2$][PF_6] (63 mg, 0.190 mmol). The mixture was stirred for 10 min resulting in a black solution. *n*-Hexane (30 cm^3) was added and the volume of the mixture was reduced *in vacuo* to induce precipitation. The product was washed with *n*-hexane (20 cm^3), giving a black powder, yield 84 mg (65%).

The complex [$Cr(CO)_2$(η-PhC≡CPh)(η-C_6Me_5H)][PF_6]·CH_2Cl_2 **1**$^+$[PF_6]$^-$·CH_2Cl_2 was prepared similarly.

[Cr(CO)(CNXyl)(η-PhC≡CPh)(η-C_6Me_6)][PF_6] 4$^+$[PF_6]$^-$. To a stirred solution of [$Cr(CO)_2$(η-PhC≡CPh)(η-C_6Me_6)][PF_6] (200 mg, 0.370 mmol) in CH_2Cl_2 (30 cm^3) was added CNXyl (60 mg, 0.454 mmol). After 1 h the solvent was reduced to low volume *in vacuo* and *n*-hexane (30 cm^3) was added. Cooling the mixture to −20 °C for 1 h gave a red-black solid, which was redissolved in CH_2Cl_2 (20 cm^3) and filtered through Celite. Addition of *n*-hexane (20 cm^3) and cooling the mixture to −20 °C for 1 d gave the product as red-black crystals, yield 148 mg (57%).

The complexes [Cr(CO){$P(OCH_2)_3CEt$}(η-PhC≡CPh)-(η-C_6Me_6)][PF_6] **5**$^+$[PF_6]$^-$ and [Cr(CO){$P(OMe)_3$}(η-PhC≡CPh)(η-C_6Me_6)][PF_6] **6**$^+$[PF_6]$^-$ were prepared similarly.

[Cr(CO)(CNXyl)(η-*p*-$MeOC_6H_4C{\equiv}CC_6H_4OMe$-*p*)-(η-$C_6Me_6$)][$PF_6$] 7$^+$[$PF_6$]$^-$. To a stirred solution of [$Cr(CO)_2$-(η-*p*-$MeOC_6H_4C{\equiv}CC_6H_4OMe$-*p*)(η-$C_6Me_6$)][$PF_6$] (110 mg, 0.168 mmol) in CH_2Cl_2 (30 cm^3) was added CNXyl (89 mg, 0.678 mmol). After 2 h, *n*-hexane (30 cm^3) was added and the volume of the solution was reduced *in vacuo*, inducing precipitation of a brown-green solid. The solid was washed with *n*-hexane (3 × 10 cm^3) and then purified to give red-black crystals, yield 148 mg (32%).

The complexes [Cr(CO)L(η-*p*-$MeOC_6H_4C{\equiv}CC_6H_4OMe$-*p*)-(η-$C_6Me_6$)][$PF_6$] {L = $P(OCH_2)_3CEt$, **8**$^+$[PF_6]$^-$, $P(OMe)_3$ **9**$^+$[PF_6]$^-$} were prepared similarly.

[Cr(CO){$P(OCH_2)_3CEt$}(η-*p*-$MeOC_6H_4C{\equiv}CC_6H_4OMe$-*p*)-(η-$C_6Me_6$)][$PF_6$]$_2$·$CH_2Cl_2$ 8^{2+}[PF_6]$_2^-$·CH_2Cl_2. To a stirred solution of [Cr(CO){$P(OCH_2)_3CEt$}(η-*p*-$MeOC_6H_4C{\equiv}CC_6H_4$-OMe-*p*)(η-$C_6Me_6$)][$PF_6$] (51 mg, 0.058 mmol) in CH_2Cl_2 (20 cm^3) was added $AgPF_6$ (15 mg, 0.058 mmol). The resulting purple solution was filtered through Celite to remove silver metal. Addition of *n*-hexane (60 cm^3) and reduction of the volume *in vacuo* induced precipitation of an oily purple solid. The complex was purified (twice) giving the product as purple microcrystals, yield 38 mg (61%).

Structure determinations of [$Cr(CO)_2$(PhC≡CPh)(η-C_6Me_5H)] 1, [$Cr(CO)_2$(PhC≡CPh)(η-C_6Me_5H)][PF_6]·CH_2Cl_2 1$^+$[PF_6]$^-$·CH_2Cl_2, [$Cr(CO)_2$(*p*-$MeOC_6H_4C{\equiv}CC_6H_4OMe$-*p*)-(η-$C_6Me_6$)][$PF_6$] 3$^+$[$PF_6$]$^-$, [Cr(CO)(CNXyl)(η-PhC≡CPh)-(η-C_6Me_6)][PF_6] 4$^+$[PF_6]$^-$, [Cr(CO){$P(OMe)_3$}(η-PhC≡CPh)-(η-C_6Me_6)][PF_6] 6$^+$[PF_6]$^-$, [Cr(CO)(CNXyl)(η-*p*-$MeOC_6H_4$-$C{\equiv}CC_6H_4OMe$-*p*)(η-C_6Me_6)][PF_6] 7$^+$[PF_6]$^-$. Red crystals of [$Cr(CO)_2$(PhC≡CPh)(η-C_6Me_5H)] **1** were grown by allowing *n*-hexane to diffuse slowly into a concentrated acetone solution of the complex at room temperature; black crystals of [$Cr(CO)_2$(PhC≡CPh)(η-C_6Me_5H)][PF_6]·CH_2Cl_2 **1**$^+$[PF_6]$^-$·CH_2Cl_2 were grown by allowing *n*-hexane to diffuse slowly into a concentrated CH_2Cl_2 solution of the salt at −20 °C; black crystals of [$Cr(CO)_2$(*p*-$MeOC_6H_4C{\equiv}CC_6H_4OMe$-*p*)-(η-$C_6Me_6$)][$PF_6$] **3**$^+$[$PF_6$] were grown by allowing *n*-hexane to diffuse slowly into a concentrated CH_2Cl_2 solution of the complex at room temperature. Crystals of [Cr(CO)(CNXyl)-(η-PhC≡CPh)(η-C_6Me_6)][PF_6] **4**$^+$[PF_6]$^-$, [Cr(CO){$P(OMe)_3$}-(η-PhC≡CPh)(η-C_6Me_6)][PF_6] **6**$^+$[PF_6]$^-$, and [Cr(CO)-(CNXyl)(η-*p*-$MeOC_6H_4C{\equiv}CC_6H_4OMe$-*p*)(η-$C_6Me_6$)][$PF_6$] **7**$^+$[$PF_6$]$^-$ were grown by allowing a concentrated solution of the complex in CH_2Cl_2 to diffuse into *n*-hexane at −20 °C.

Many of the details of the structure analyses of **1**, **1**$^+$[PF_6]$^-$·CH_2Cl_2, **3**$^+$[PF_6]$^-$, **4**$^+$[PF_6]$^-$, **6**$^+$[PF_6]$^-$ and **7**$^+$[PF_6]$^-$ are listed in Table 4. The structures of **1** and **1**$^+$[PF_6]$^-$·CH_2Cl_2 have been re-refined from the data published in ref. 2 (CCDC refcodes RAPCEQ and RAPCIU) and the atoms have been renumbered for consistency with the other structures reported herein.

All hydrogen atoms were assigned isotropic displacement parameters and were constrained to ideal geometries, with the exception of the hydrogens on C(12) of **1** which were attached in two positions rotated from each other by 60° and with occupancy factors fixed at 0.5. The absolute structure of **1**$^+$[PF_6]$^-$·CH_2Cl_2 was confirmed by the Flack parameter, estimated at −0.08(4). Refinements converged to the residuals

Table 4 Crystal and refinement data for arenechromium alkyne complexes

Compound	**1**	$\mathbf{1}^{+}[PF_6]^{-}\cdot CH_2Cl_2$	$\mathbf{3}^{+}[PF_6]^{-}$	$\mathbf{4}^{+}[PF_6]^{-}$	$\mathbf{6}^{+}[PF_6]^{-}$	$\mathbf{7}^{+}[PF_6]^{-}$
Formula	$C_{27}H_{26}CrO_2$	$C_{28}H_{28}Cl_2CrF_6O_2P$	$C_{30}H_{32}CrF_6O_4P$	$C_{36}H_{37}NCrF_6OP$	$C_{30}H_{37}CrF_6O_4P_2$	$C_{38}H_{41}NCrF_6O_3P$
M	434.48	664.37	653.53	696.64	689.54	756.69
Crystal system	Triclinic	Monoclinic	Monoclinic	Monoclinic	Orthorhombic	Monoclinic
Space group (no.)	$P\bar{1}$ (2)	$P2_1$ (4)	$P2_1/c$ (14)	$P2_1/c$ (14)	$Pbca$ (61)	$P2_1/n$ (14)
a/Å	7.1132(14)	9.1866(19)	8.9707(18)	11.140(2)	16.993(4)	11.1760(17)
b/Å	9.353(3)	15.768(3)	18.592(4)	13.4946(15)	26.514(6)	22.284(5)
c/Å	16.781(3)	9.913(3)	17.104(3)	22.153(3)	28.425(8)	14.739(2)
α/°	88.5(2)	90	90	90	90	90
β/°	81.84(16)	100.83(16)	97.00(3)	99.082(9)	90	104.917(12)
γ/°	72.0(2)	90	90	90	90	90
T/K	173	173	293	173	173	173
U/Å^{-3}	1050.6(4)	1410.4(5)	2831.4(10)	3288.7(8)	12807(5)	3547.1(10)
Z	2	2	4	4	16	4
μ/mm^{-1}	0.566	0.717	0.536	0.461	0.526	0.437
Reflections collected	4987	6858	10012	17130	62123	18328
Independent reflections (R_{int})	3518 (0.0205)	3808 (0.0543)	3920 (0.0577)	5777 (0.0456)	10056 (0.2230)	6232 (0.0469)
Final R indices [$I > 2\sigma(I)$]: R_1, wR_2	0.0281, 0.0732	0.0553, 0.1243	0.0574, 0.1312	0.0451, 0.1026	0.0643, 0.1244	0.0582, 0.1227

given in Table 4. The best crystal of $\mathbf{6}^{+}[PF_6]^{-}$ available for structure determination was weakly diffracting with poor peak profiles, leading to the large value of R_{int}.

CCDC reference numbers 189051–189056.

See http://www.rsc.org/suppdata/dt/b2/b206177p/ for crystallographic data in CIF or other electronic format.

Acknowledgements

We thank the EPSRC for studentships (D. J. H., O. D. H. and M. J. Q.) and a Postdoctoral Research Associateship (C. J. A.), and the University of Bristol for a Postgraduate Scholarship (I. M. B.).

References

1 (*a*) K. Broadley, N. G. Connelly, G. A. Lane and W. E. Geiger, *J. Chem. Soc., Dalton Trans.*, 1986, 373; (*b*) C. Coates, N. G. Connelly and M. C. Crespo, *J. Chem. Soc., Dalton Trans.*, 1988, 2509; (*c*) R. P. Aggarwal, N. G. Connelly, M. C. Crespo, B. J. Dunne, P. M. Hopkins and A. G. Orpen, *J. Chem. Soc. Dalton Trans.*, 1992, 655; (*d*) N. G. Connelly, T. Escher, A. J. Martin, B. Metz and A. G. Orpen, *J. Cluster Sci.*, 1995, **6**, 125; (*e*) N. G. Connelly, W. E. Geiger, M. C. Lagunas, B. Metz, A. L. Rieger, P. H. Rieger and M. J. Shaw, *J. Am. Chem. Soc.*, 1995, **117**, 12202; (*f*) N. G. Connelly, W. E. Geiger, S. R. Lovelace, B. Metz, T. J. Paget and R. Winter, *Organometallics*, 1999, **18**, 3201; (*g*) I. M. Bartlett, S. Carlton, N. G. Connelly, D. J. Harding, O. D. Hayward, A. G. Orpen, C. D. Ray and P. H. Rieger, *Chem. Commun.*, 1999, 2403; (*h*) C. J. Adams, N. G. Connelly and P. H. Rieger, *Chem. Commun.*, 2001, 2458.

2 I. M. Bartlett, N. G. Connelly, A. G. Orpen, M. J. Quayle and J. C. Rankin, *Chem. Commun.*, 1996, 2583.

3 M. P. Castellani, N. G. Connelly, R. D. Pike, A. L. Rieger and P. H. Rieger, *Organometallics*, 1997, **16**, 4369.

4 C. J. Adams, K. M. Anderson, N. G. Connelly, D. J. Harding, O. D. Hayward, A. G. Orpen, E. Patron and P. H. Rieger, *Chem. Commun.*, 2002, 130.

5 W. Strohmeier and H. Hellmann, *Chem. Ber.*, 1965, **98**, 1598.

6 N. G. Connelly and G. A. Johnson, *J. Organomet. Chem.*, 1974, **77**, 341.

7 M. A. Bennett, G. A. Heath, D. C. R. Hockless, I. Kovacik and A. C. Willis, *Organometallics*, 1998, **17**, 5867.

8 N. G. Connelly, B. Metz, A. G. Orpen and P. H. Rieger, *Organometallics*, 1996, **15**, 729.

9 M. A. Bennett, G. A. Heath, D. C. R. Hockless, I. Kovacik and A. C. Willis, *J. Am. Chem. Soc.*, 1998, **120**, 932.

10 (*a*) J. Chatt and L. A. Duncanson, *J. Chem. Soc.*, 1953, 2939; (*b*) M. J. S. Dewar, *Bull. Soc. Chim. Fr.*, 1951, **18**, C71.

11 J. L. Templeton, J. L. Caldarelli, S. Feng, C. C. Philipp, M. B. Wells, B. E. Woodworth and P. S. White, *J. Organomet. Chem.*, 1994, **478**, 103.

12 B. E. R. Schilling, R. Hoffmann and D. L. Lichtenberger, *J. Am. Chem. Soc.*, 1979, **101**, 585.

13 J. L. Templeton, P. B. Winston and B. C. Ward, *J. Am. Chem. Soc.*, 1981, **103**, 7713.

14 A. G. Orpen and N. G. Connelly, *Organometallics*, 1990, **9**, 1206.

15 B. E. R. Schilling, R. Hoffmann and J. W. Faller, *J. Am. Chem. Soc.*, 1979, **101**, 592.

16 N. G. Connelly, A. G. Orpen, A. L. Rieger, P. H. Rieger, C. J. Scott and G. M. Rosair, *J. Chem. Soc., Chem. Commun.*, 1992, 1293.

17 I. M. Bartlett, N. G. Connelly, A. J. Martín, A. G. Orpen, T. J. Paget, A. L. Rieger and P. H. Rieger, *J. Chem. Soc., Dalton Trans.*, 1999, 691.

18 R. D. Pike, A. L. Rieger and P. H. Rieger, *J. Chem. Soc., Faraday Trans. 1*, 1989, **85**, 3913.

19 J. R. Morton and K. F. Preston, *J. Magn. Reson.*, 1978, **30**, 577.

20 B. Nicholls and M. C. Whiting, *J. Chem. Soc.*, 1959, 551.

21 N. G. Connelly and W. E. Geiger, *Chem. Rev.*, 1996, **96**, 877.